Computation & theory

First-principles investigations of structural, optoelectronic and thermoelectric properties of Cu-based chalcogenides compounds

Merieme Benaadad[1,*] (iD), Abdelhakim Nafidi[1], Samir Melkoud[1], Muhammad Salman Khan[2], and Driss Soubane[1]

[1] *Laboratory of Condensed Matter Physics and Nanomaterials for Renewable Energy, University Ibn Zohr, 80000 Agadir, Morocco*
[2] *Department of Physics, Abdul Wali Khan University, Mardan 23200, Pakistan*

ABSTRACT

The structural, electronic, optical and thermoelectric properties of copper-based ternary chalcogenides $ACuSe_2$ (A = Sc, Y and La) were investigated within the framework of the density functional theory (DFT). The electronic band structures and density of states exhibit that $ScCuSe_2$ and $YCuSe_2$ have the indirect band gaps, while $LaCuSe_2$ displays a direct band gap-type transition. The band structure calculations agree well with other results in the literature. The optical behavior of the studied materials was analyzed in terms of dielectric functions, refractive index, extinction coefficient, absorption coefficient, optical conductivity, reflectivity and energy loss factor. The refractive indices increase to the maximum values of 4.4, 4 and 4.1 at the short infrared and visible wavelengths for $ScCuSe_2$, $YCuSe_2$ and $LaCuSe_2$, respectively. Then, they decrease to get a value below 1.0 at the UV wavelengths. Moreover, the material response with temperature was investigated by Seebeck coefficient, figure of merit, specific heat capacity, power factor, thermal conductivity and susceptibility. The high Seebeck effect and large power factor values confirm the efficiency of these materials in thermoelectric energy converter technology. Among the three studied ternary materials, $YCuSe_2$ has the highest value of dimensionless figure of merit of 0.45 at room temperature. These results would probably provide a new route to the experimentalists for the potential usage and applications of $ScCuSe_2$, $YCuSe_2$ and $LaCuSe_2$ in thermoelectric and optoelectronic devices.

Introduction

To get an essential growth in the energy production, new technological devices are required specifically, in the field of photovoltaics and thermoelectric technology [1–3]. The most common materials studied for this purpose include cadmium telluride, gallium arsenide, copper indium diselenide, nitrides, oxides and organic materials. Such materials were studied practically for the solar energy conversion [4–7]. Several high-figure-of-merit (ZT) thermoelectric materials were reviewed by Wei et al. [8]; many copper chalcogenide materials possessed attractive performance such $Cu_{2-2x}Ag_{2x}Se_{1-x}S_x$; a ZT value of 1.6 was obtained in the $Cu_{1.8}Ag_{0.2}Se_{0.9}S_{0.1}$ sample at 900 K [9]. The importance of the thermoelectric materials with low thermal conductivity is their use in water evaporation systems which are energy effective, with efficiencies ranging from 60 to over 90% [10]. There is a variety of solar water evaporation systems based on biomass and other natural products such wood and plants which have been investigated in different forms; their original shape allows them to be used as photothermal surfaces for the leaves [10]. Perovskite solar cells have also emerged as a promising and highly efficient solar technology. A recent study by Doolin et al. [11] presents a methodology for green solvent selection; it shows demonstrate the application of green chemistry principles to solvent selection for perovskite photovoltaic manufacturing. Building integrated photovoltaics and smart windows have gained considerable research attention, due to their promising prospects in terms of energy production from renewables. The use of cobalt redox electrolytes in partly covered photoelectrochromic devices was investigated experimentally by Dokouzis et al. [12] The result devices exhibited rather good transparency in the bleach. Furthermore, sustainable solar energy harvesting technologies able to provide enhanced performance under low irradiation are highly suited as complementary renewable sources to Si-based photovoltaics from a smart-grid energy perspective. Among them, dye-sensitized solar cells (DSSCs) are one of the most interesting choices [13].

Previously, some binary-type chalcogenides were of interest for the thermoelectric applications, such as Bi_2Te_3 lead telluride, inorganic clathrates, oxides and perovskite solar cells [14–19]. Synthesis of such ternary and quaternary chalcogenide materials with an increasingly complex composition becomes a principal direction in modern science of materials [20]. These ternary chalcogenides are mostly semiconductor materials with energy band gaps ranging from 0.6 to 4.0 eV [21]. The basic applications of these materials include light-emitting diodes (LED), infrared materials, the fabrication of solar energy converters, nonlinear optical tools and field-effect transistors [22–24]. Nonlinear optical devices provide a means of extending the frequency range of available laser sources. $LiInSe_2$ and $LiIn(S_{0.5}Se_{0.5})_2$ crystals among the most effective crystals for the creation of middle IR optical parametric oscillators and difference frequency generators under pumping by all-solid-state and common near-IR lasers [25]. Numerous new effective ternary sulfides and binary selenides highly nonlinear optical (NLO) have been compiled and classified for optoelectronic device applications by Atuchin et al. [26] as $HgGa_2S_4$ which investigated experimentally with X-ray photoelectron spectroscopy [27]. The silver chalcogenides are promising superionic semiconductors with low heat conductivity of the lattice as the Ag_2Se–Ho_2Se_3 compound [28]. The high potential of $LiGaTe_2$ for the optical frequency conversion in the mid-IR spectral range has been demonstrated in several studies [29]. These results indicate that $LiGaTe_2$, besides its well-known pronounced linear and nonlinear optical properties in IR spectral range, possesses the specific structural effects. A recent investigation on the electronic, optical and thermoelectric properties of nine ternary chalcogenides, $NaAX_2$, where A = As, Sb, Bi and X = S, Se, Te was carried out using DFT calculations. Their band gaps ranged from 0.51 to 1.95 eV. The estimation of thermoelectric parameters showed high Seebeck coefficients of 500 and 300 $\mu V/K$ for $NaSbS_2$ and $NaSbSe_2$ at 600 K, respectively. These results suggest that these two compounds are potential candidates for photovoltaic structures, especially in tandem solar cells, and thermoelectric applications [30].

Among the family of the copper-based, ternary and quaternary semiconductor compounds are the most widely used as absorbers materials in thin film solar cells, due to their unique structural and photoelectric properties [31, 32]. Moreover, $Cu_2ZnSn(S,Se)_4$ (CZTSSe) is also an interesting absorber material for thin film solar cells, which could replace the current absorber layers like $Cu(In, Ga)(S,Se)_2$ (SIGSSe) and

CdTe. In this context, a detailed study of band alignment parameters at the interface of n-type MZO and p-type CZTSSe system was investigated by Sengar et al. [33], a Cd-free n-type buffer layers with two different Mg-doped ZnO layers ($Mg_{0.26}Zn_{0.74}O$, $Mg_{0.30}Zn_{0.70}O$) have been examined using ultraviolet photoelectron spectroscopy. In addition, a very recent study was carried about improving the $Cu_2ZnSn(S,Se)_4$-based photovoltaic conversion efficiency by back-contact modification having a low toxicity, natural abundance, outstanding light absorption, and higher theoretical efficiency [33, 34].

The ternary compounds such as $CuInSe_2$, $CuAlSe_2$ and $CuGaSe_2$ [35–38] have also attracted the attention of researchers. The scarcity of both indium (In) and gallium (Ga) increases their cost, and, thus, using these elements as absorbers materials increases the cost of solar cells and limits their wide application in copper indium gallium selenide solar cell (CIGSS) [39]. Instead of In and Ga, which are group IIIB members, the group IIIA elements like Y and Sc can be employed. The chalcogenides containing Y and Sc have a unique electronic structure, a high quantum absorption at shorter wavelengths and subsequently emit light at longer wavelengths [40–42]. The structure and electronic properties of $CuScS_2$ semiconductor were reported by Scanlon et al. [43]using the hybrid density functional theory. The optoelectronic and elastic properties of $CuYS_2$ were studied by Brik et al. [44], using the first-principles methods. They found band gaps of 1.34 and 1.38 eV by the potential generalized gradient approximation (GGA) and local-density approximation (LDA), respectively. The synthesis and single-crystal structure determination of $LaCuSe_2$ were reported by Julien-Pouzol [45].

A promising series of ternary chalcogenide materials is $ACuSe_2$, where A = Y, Sc, La. Among these materials, yttrium copper diselenide ($YCuSe_2$) is a candidate for solar cell applications. Its lifetime is smaller than that in materials made with silicon. It is a cheap compound with low toxicity [46]. Regarding the compounds interest, Ruixin et al. [46] prepared $YCuSe_2$ using self-propagating high-temperature synthesis method at 1016.2 °C. They found that it was a promising photovoltaic material with an experimental optical gap of 1.53 eV. Similarly, Rugut et al. [47] analyzed the thermoelectric and transport proprieties of $YCuSe_2$. The study showed that it has potential applications as thermoelectric devices. Although a few groups of researchers have explored

thermoelectric properties of $YCuSe_2$, there exists scarce information concerning $ScCuSe_2$ and $LaCuSe_2$ materials. Trigonal phase of $ScCuSe_2$ was briefly explored experimentally by Pouzol, Guiltard et al. [48] reporting the structural stability, lattice constants and density.

To the best of our knowledge, rare theoretical or experimental investigations exist about the electronic structures, optical and thermoelectric proprieties of $ScCuSe_2$, $YCuSe_2$ and $LaCuSe_2$ (Fig. 1). In this work, we focus on the electronic band structure, density of states, optical and thermoelectric properties of these three compounds using the density functional theory (DFT) methods. We calculated the electronic band structure, density of states, optical and thermoelectric properties of these three compounds using the density functional theory (DFT). The manuscript is organized as follows. The details of our calculations are reported in "Computational details" section. In "Result and discussion" section, the structural, electronic, optical as well as the thermoelectric properties of examined materials are discussed. In "Conclusion" section, we summarize the conclusions of the study and perspectives.

Computational details

We used here the density functional theory (DFT), which is one of the most accurate theories to calculate the electronic structure of solid materials. This technique is increasingly used as an exploratory tool for material discovery and in computational experiments [49]. DFT simulation codes can calculate a vast range of structural, chemical, optical, spectroscopic, elastic, vibrational, and thermodynamic phenomena [50–53]. The ability to predict structure–property relationships has revolutionized experimental fields, such as vibrational and solid-state NMR spectroscopy. In semiconductor physics, great progress has been made in the electronic structure of bulk and defect states despite the severe challenges presented by the description of excited states. DFT is increasingly used as an exploratory tool for materials discovery and computational experiments, culminating in ex nihilo crystal structure prediction [54, 55].

All the calculations achieved in this work were performed using the full potential linearized augmented plane wave (FP-LAPW) in addition to local orbitals method as developed in the WIEN2k code
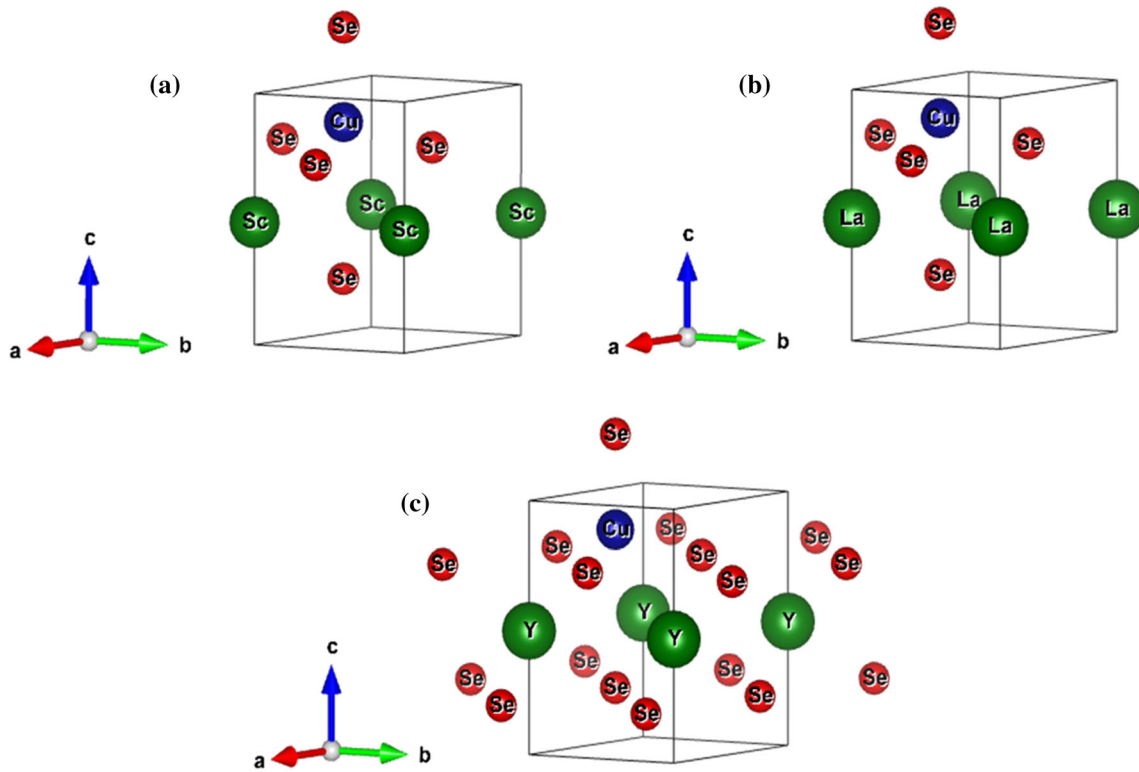
Figure 1 Calculated unit cell structures for **a** ScCuSe$_2$, **b** LaCuSe$_2$, **c** YCuSe$_2$, respectively.

[56]. The LDA along with PBE-GGA [57] approximations is used to described the exchange correlation potentials that calculate the total energy and are actually based on optimization of the exchange correlation energy. Furthermore, to obtain accurate electronic band structures, we used the recently modified Becke–Johnson potential (m-BJ) [58]. The space was divided into two parts: the spherical muffin-tin region around the nucleus where the radial solutions of the Schrödinger wave equation and its energy derivative were used as basic functions, and the interstitial muffin-tin region, where the base set consisted of plane waves. We selected RMT reduction by 5% so lattice parameters could optimize finely. The atomic sphere radii were selected to be 2.5 a.u., 2.34 a.u. and 2.23 a.u. for A = (Sc, Y, La), Cu, and Se, respectively, for each element of the compounds, i.e., ScCuSe$_2$, YCuSe$_2$ and LaCuSe$_2$. The Brillouin zone integration is performed using a mesh of 500 k-points with $R_{MT} K_{max} = 8$ (a.u)$^{-1}$, where R_{MT} indicates the smallest muffin-tin radius and K_{max} is the maximum size of reciprocal lattice vector, in addition to the Gaussian parameter $G_{max} = 12$. We further fixed the Gaussian smearing value of 0.1 eV

to get converged and much accurate electronic density of states, in addition to the convergence energy of 0.0001 Ry to get stability of the system within self-consistent calculations.

The optical properties of a material are described using the real $\varepsilon_1(\omega)$ and imaginary $\varepsilon_2(\omega)$ parts of the complex dielectric function given by the expression:

$$\varepsilon(\omega) = \varepsilon_1(\omega) + i\varepsilon_2(\omega) \tag{1}$$

where $\varepsilon_1(\omega)$ corresponds to dispersion of photons and $\varepsilon_2(\omega)$ is associated with the energy absorption of the material. The imaginary part of the complex dielectric function can be calculated using the following relation:

$$\varepsilon_2(\omega) = \frac{2\pi e^2}{\Omega \varepsilon_o} \sum_{c,v} \sum_{k} \left| \psi_k^c |ur| \psi_k^v \right|^2 \delta \left(E_k^c - E_k^v - h\omega \right) \tag{2}$$

where Ω is unit cell volume, the valence and conduction band are denoted by (v, c), respectively, the ω term is the incident light frequency, and k defines the direction of polarization of the E field with a full isotropic type average value in the polycrystalline materials. Based on the complex dielectric function, we calculated the significant optical parameters such

as the reflectivity $R(\omega)$, absorption coefficient $I(\omega)$, refractive indices $n(\omega)$, energy loss spectrum $L(\omega)$, extinction coefficient $k(\omega)$ and real optical conductivity $\sigma^{\text{real}}(\omega)$ by the given relations [59].

$$L(\omega) = \frac{\varepsilon_2(\omega)}{\varepsilon_1^2(\omega) + \varepsilon_2^2(\omega)} \tag{3}$$

$$I(\omega) = \frac{\sqrt{2}\omega}{c}\left(\sqrt{\varepsilon_1^2(\omega) + \varepsilon_2^2(\omega)} - \varepsilon_1(\omega)\right)^{\frac{1}{2}} \tag{4}$$

$$R(\omega) = \left|\frac{\sqrt{\varepsilon_1(\omega) + i\varepsilon_2(\omega)} - 1}{\sqrt{\varepsilon_1(\omega) + i\varepsilon_2(\omega)} + 1}\right|^2 \tag{5}$$

$$n(\omega) = \left(\frac{1}{2}\left[\sqrt{\varepsilon_1^2(\omega) + \varepsilon_2^2(\omega)} + \varepsilon_1(\omega)\right]\right)^{\frac{1}{2}} \tag{6}$$

$$k(\omega) = \left(\frac{1}{2}\left[\sqrt{\varepsilon_1^2(\omega) + \varepsilon_2^2(\omega)} - \varepsilon_1(\omega)\right]\right)^{\frac{1}{2}} \tag{7}$$

$$\sigma^{\text{real}}(\omega) = \varepsilon_0(\omega)\varepsilon_1(\omega) \tag{8}$$

We have calculated also the thermoelectric proprieties, including thermal conductivity, Seebeck coefficient, specific heat capacity, power factor, electrical susceptibility and figure of merit, with the use the BoltzTrap code [60].

Result and discussion

Structural proprieties

The unit cell structure of our studied copper-based ternary chalcogenides ($ACuSe_2$) is presented in Fig. 1. We show in Table 1 the computed values of lattice constants and volumes alongside the available theoretical and experimental values where possible. For the case of $ScCuSe_2$, its trigonal form has been explored experimentally by Pouzol and Guiltard where in both structural stability, lattice constants

and densities are reported in [48]. While investigating the interactions between the components in the Y_2Se_3-Cu_2Se-$SnSe$ and Y_2Se_3-Cu_2Se-$PbSe$ system at 870 K determined using X-ray powder diffraction, Shemet et al. [61] confirmed the existence of the trigonal $YCuSe_2$ in the Cu_2ErS_2 structure having lattice constants as provided in Table 1. For $LaCuSe_2$, our calculated structural parameters agree reasonably with experimentally reported in [62]. Hence, all the calculated structural properties agree reasonably well with previous results and experimental data. Furthermore, employing the (PBE-GGA) generalized gradient approximation we optimized the atomic positions using the minimized forces which act on atoms. The atomic coordinates and isotropic temperature factors are given in Table 2.

Band structure and density of states

The study of material band structure is very essential as it gives information about optoelectronic behavior at different frequency excitations, i.e., electron and hole transitions, and permits to examine the electronic properties. In addition, for technological applications of semiconductors, the nature of band structure is a key parameter, and it can be measured experimentally or determined theoretically. We calculated the electronic band structures (EBS) of the three materials along the high-symmetry directions, as displayed in Fig. 2. For the $ScCuSe_2$ and $YCuSe_2$ compounds, the valence band maximum and conduction band minimum are located at different points (Γ and M) of the first Brillion zone (FZB) resulting in an indirect band gaps (Γ-M) of 0.7 and 1.2 eV, respectively, while $LaCuSe_2$ exhibits a direct band transition with a band gap value ($\Gamma v - \Gamma c$) of 0.8 eV. So, the indirect band gap increases from A = Sc (0.7 eV) to Y (1.2 eV) and then decreases to direct band gap for La (0.8 eV). The maximum band

Table 1 The main parameters of processing and refinement

Compound	Space group	a (Å)	b (Å)	c (Å)	α (°)	β (°)	γ (°)	V (Å³)
$ScCuSe_2$	P3m1	3.944	3.944	6.292	90	90	120	84.800
		3.730 [48]	3.730	6.098	90	90	120	84.840
$YCuSe_2$	P3m1	4.097	4.097	6.450	90	90	120	93.777
		4.070 [61]	4.070	6.460	90	90	120	107.009
$LaCuSe_2$	P2₁/c	7.267	6.848	7.610	90	90	90.073	378.776
		6.81	7.58	7.20		97.12		371.662

Table 2 Atomic coordinates and isotropic temperature factors for the ACuSe$_2$ compounds

Atom	x	y	z	Occupation	B	Site	Symmetry
ScCuSe$_2$							
Sc1	0.0	0.0	0.0	1.0	1.0	1a	3 m
Cu1	0.333	0.666	0.609	1.0	1.0	1b	3 m
Se1	0.333	0.666	0.225	1.0	1.0	1b	3 m
Se2	0.666	0.333	0.740	1.0	1.0	1c	3 m
YCuSe$_2$							
Y1	0	0	0	1.0	1.0	1a	3 m
Cu1	0.666	0.333	0.386	1.0	1.0	1c	3 m
Se1	0.333	0.666	0.273	1.0	1.0	1b	3 m
Se2	0.666	0.333	0.763	1.0	1.0	1c	3 m
LaCuSe$_2$							
La1	0.298	0.691	0.950	1.0	1.0	4e	1
La2	0.201	0.308	0.450	1.0	1.0	4e	1
La3	0.701	0.308	0.049	1.0	1.0	0	
La4	0.798	0.691	0.549	1.0	1.0	0	
Cu1	0.544	0.067	0.661	1.0	1.0	4e	1
Cu2	0.955	0.932	0.161	1.0	1.0	4e	1
Cu3	0.455	0.932	0.338	1.0	1.0	0	
Cu4	0.044	0.067	0.838	1.0	1.0	0	
Se1	0.001	0.411	0.774	1.0	1.0	4e	1
Se2	0.498	0.588	0.274	1.0	1.0	4e	1
Se3	0.998	0.588	0.225	1.0	1.0	0	
Se4	0.501	0.411	0.725	1.0	1.0	0	
Se5	0.721	0.905	0.887	1.0	1.0	4e	1
Se6	0.778	0.094	0.387	1.0	1.0	4e	1
Se7	0.278	0.094	0.112	1.0	1.0	0	
Se8	0.221	0.905	0.612	1.0	1.0	0	

gap is observed for A = Y (1.2 eV). The decrease of the band-gap value from LaCuSe$_2$ or ScCuSe$_2$ to YCuSe$_2$ can be accredited due to the shift related to conduction bands toward Fermi level that most likely reflects the significance of La and Sc in band gap opening if the corresponding valence band is allowed to be unchanged.

The band gaps for the examined materials were calculated using the modified Becke–Johnson exchange potential (mBJ). The obtained values of the fundamental gap of ScCuSe$_2$ using PBE and hybrid exchange functional (HSE06) are 0.65 and 1.62 eV, respectively [41]. It can be observed that the theoretical DFT-based calculation of PBE and mBJ characteristically underestimate corresponding band-gap than HSE06. Hence, according to this calculation and previously reported values of ScCuSe$_2$ band gaps, the most optimal value can range from 0.65 to 0.7 eV. The band gap of YCuSe$_2$ calculated in the present study is comparable to the experimental optical gap that was estimated to be 1.53 eV using self-propagating high-temperature synthesis method [46].

Other DFT calculation confirms that YCuS$_2$ has indirect band gap with a value of 1.3 eV for theoretical bulk modulus of 70 GPa, as computed using the PBE functional [44]. The PBE-DFT gap was computed to be 1.08 eV [47]. The presence of the fundamental band gap energy between valence and conduction bands indicates the semiconductor behavior for the three examined materials.

So, as to explain further the contributions related to the various electronic states in both valence and conduction bands, we also computed the density of states. In Fig. 3a, b and c, the total density of states (TDOS) and atomic-projected density of states (PDOS, in states/eV) are presented for the studied compounds. As seen, TDOS for the three materials is nearly similar due to the similarity in chemical bonding. In the case of valence band, TDOS of ScCuSe2 is divided into two parts: the first one situated in the region from − 14.1 to − 12.2 eV and the
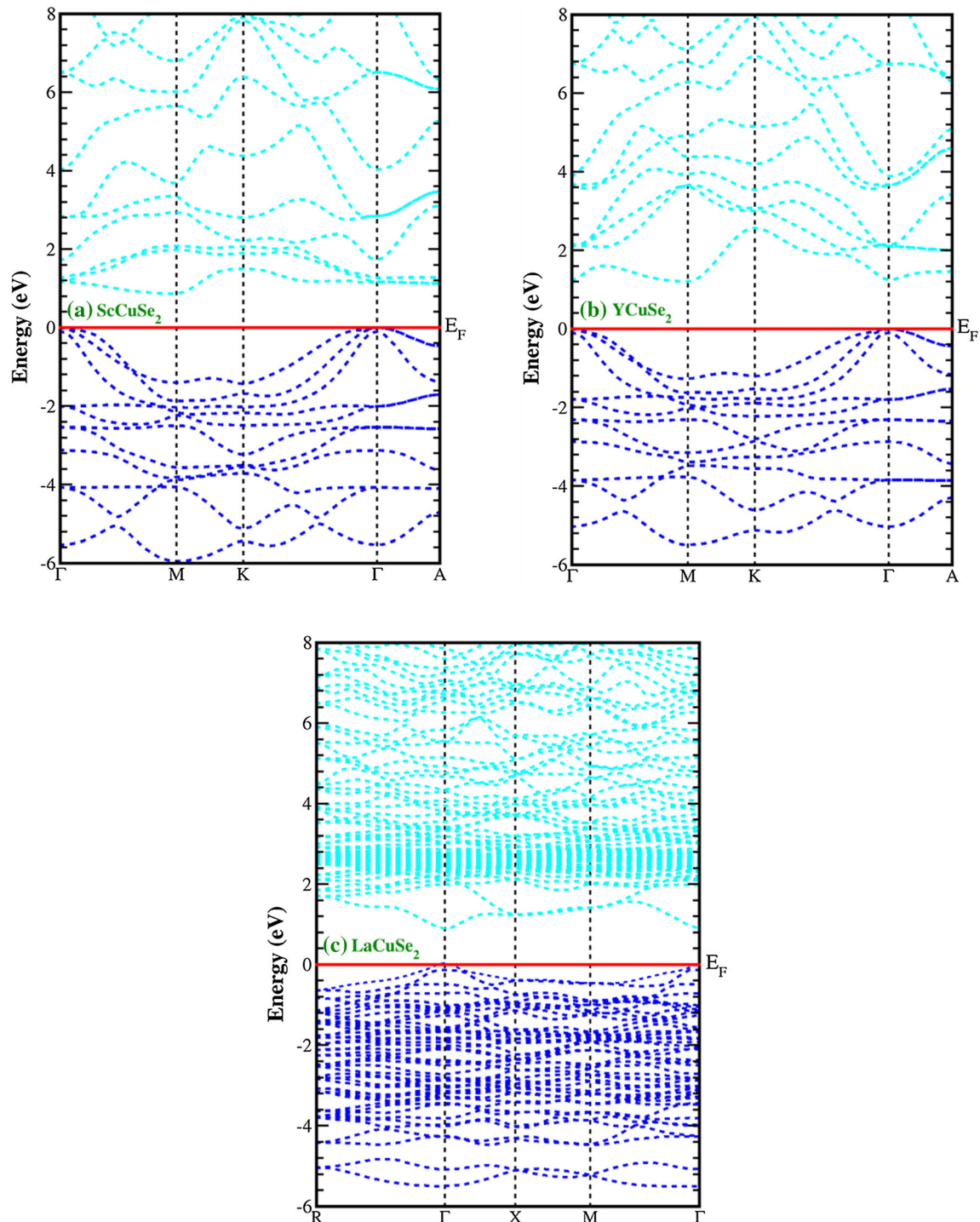
Figure 2 Calculated band structures for **a** ScCuSe$_2$, **b** YCuSe$_2$, **c** LaCuSe$_2$, respectively.

large region ranges from -6.2 to 0.01 eV; in this region, we see the dominance of Tot-Cu while DOS of other elements is negligible. As seen, for this material, the principal contribution is through the DOS components Se-p (2 states/eV), Cu-d and Sc-p which gives a strong support to the partial density of states, while DOS of other elements is negligible. In the conduction band, DOS shows a large contribution range from 0.6 to 15 eV which is supported, especially by Sc-d, Se-p and Cu-p. For YCuSe2, there is the
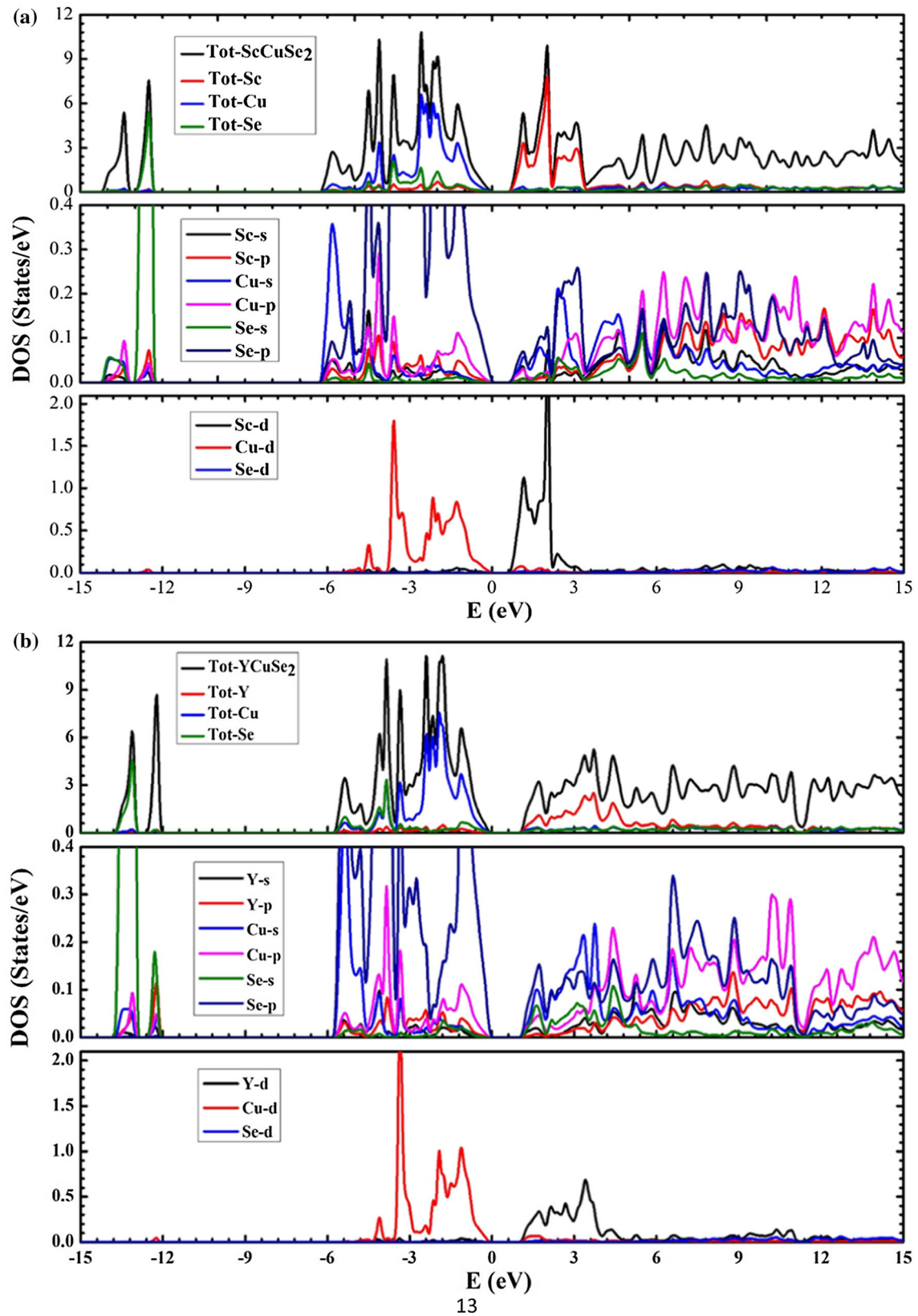
Figure 3 Calculated total and partial density of states for **a** ScCuSe$_2$, **b** YCuSe$_2$, and **c** LaCuSe$_2$.
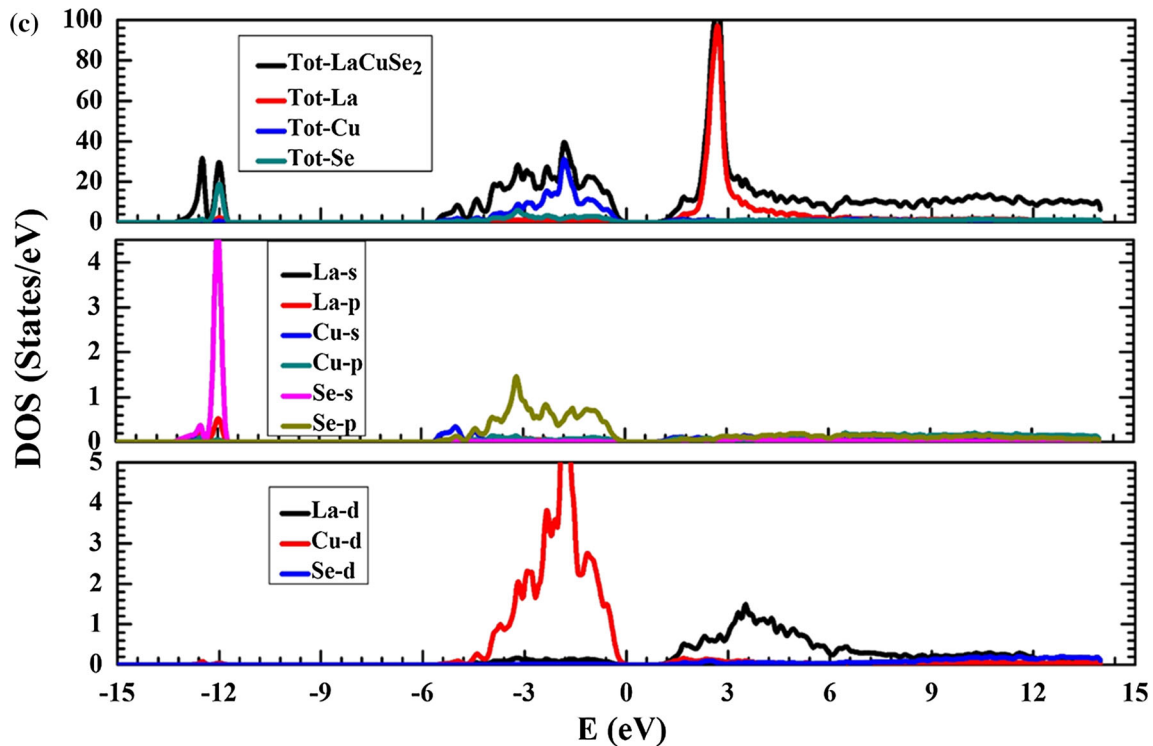
(c)

Figure 3 continued.

large contribution in the case of the valence band ranging from − 5.7 to 0 eV, and it is due to the Se-p and Cu-d states, while the conduction band consists mostly of Y-p, Cu-p and Se-p states with a small contribution of all other elements. For the last material LaCuSe2, in the valence band, DOS, divided into three parts, consisting of La-p, Se-s and Se-p states, while in the case of conduction band, which lies between 2.2 and 15 eV, a major contribution is from La-d with 1.5 states/eV.

Optical proprieties

In this section, the optical parameters are calculated in the energy range of 0–14 eV. We calculated the dielectric functions ε_1 and ε_2 of the investigated compounds as a function of the photon energy, as shown in Fig. 4a, b, respectively. As seen in Fig. 4a, the real part of dielectric function $\varepsilon_1(\omega)$ increases from $\varepsilon_1(0)$ to reach a maximum value at 1.3, 1.9 and 1.8 eV for ScCuSe$_2$, YCuSe$_2$ and LaCuSe$_2$, respectively, and, then, it begins decreasing to negative values that show the reflection of light falling on the material surface and materials become metallic [63]. The zero limits of frequency for ScCuSe$_2$, YCuSe$_2$ and

LaCuSe$_2$ are present at 6.6, 6.7 and 5.4 eV, respectively.

As we can see that the three curves remain constant from $\varepsilon_1(- 1.4)$ at 8.9 eV. The peaks observed mainly in the three materials are due to the transitions from the valence band top to the conduction band bottom. It is deduced that these values of the dielectric constants for the three materials have an inverse relationship with their corresponding band gaps due to the negative energy ranges.

In Fig. 4b, the imaginary part of dielectric function, $\varepsilon_2(\omega)$, is shown. The principal peaks of the optical critical point are 13, 11.8 and 12 for ScCuSe$_2$, YCuSe$_2$ and LaCuSe$_2$, respectively, which correspond to their energy values of 1.8, 2.3 and 3 eV. From the imaginary part of dielectric constant, we calculated the frequency-dependent absorption coefficient $I(\omega)$, as shown in Fig. 4c. For all the three materials, the absorption spectra start increasing nearly at 1 eV to reach some maxima at 9.1, 7.7 and 7.2 eV for ScCuSe$_2$, YCuSe$_2$ and LaCuSe$_2$, respectively, and, then, it continues increasing hardly in the range from 9.4 to 13.5 eV.

One of the most important optical parameters is the electron energy loss function $L(\omega)$, because it permits
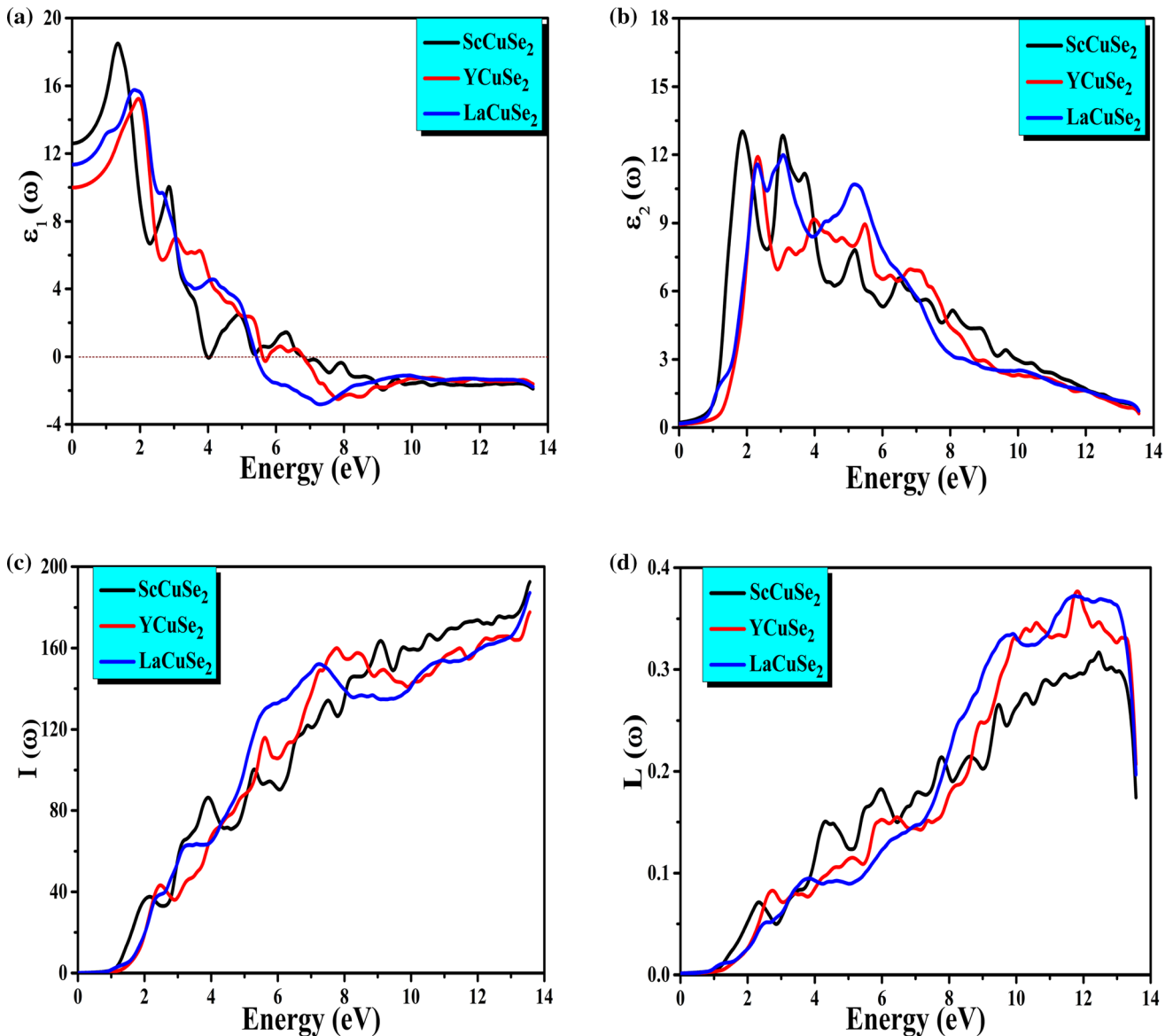
Figure 4 Calculated **a** real component, **b** imaginary component of dielectric function, **c** absorption coefficient $I(\omega)$, **d** energy loss function $L(\omega)$, for $ACuSe_2$, respectively.

to measure the propagation loss of energy inside the solid materials. As shown in Fig. 4d, $L(\omega)$ starts increasing from 1 eV for the three materials to get the maximum peaks at 12.4, 11.8 and 11.7 eV for $ScCuSe_2$, $YCuSe_2$ and $LaCuSe_2$, respectively. These peaks in the $L(\omega)$ spectra are called to be plasma resonance, and they are due to the lost energy when the incident photon energy is higher than E_g of material. After that, the energy loss function declines rapidly for the three materials.

In Fig. 5a, the calculated reflectivity spectra $R(\omega)$ are displayed for the three materials. The zero frequency limits are about 0.31, 0.25 and 0.29 for

$ScCuSe_2$, $YCuSe_2$ and $LaCuSe_2$, respectively. The maximum of peaks for the three materials is situated in the energy range of 7.2–9.4 eV. The sharp peaks of $ScCuSe_2$ and $YCuSe_2$ show that these materials can be used as shielding materials against UV radiations. In Fig. 5a, a sharp increase is seen from 12 to 13.5 eV for the three materials. In Fig. 5b, the real part of the optical conductivity is plotted. It starts increasing at 0.9 eV for the three materials and reach high peak values at 6.6, 5.5 and 5.3 eV in $ScCuSe_2$, $YCuSe_2$ and $LaCuSe_2$, respectively. A sharp decrease of the spectra in the range of 10 to 13.5 eV can be also seen. The refractive index $n(\omega)$ is plotted in Fig. 5c. It starts
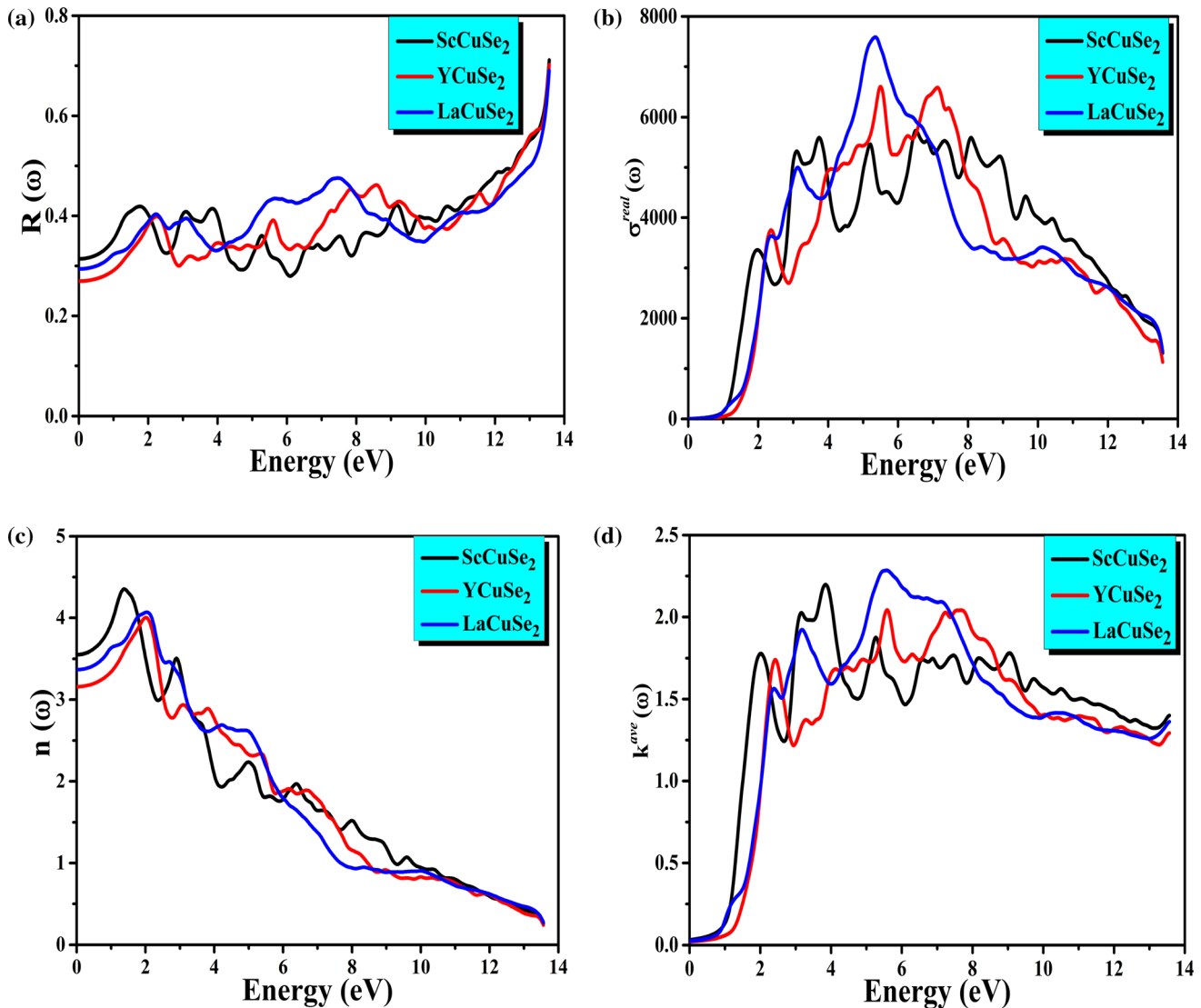
Figure 5 Calculated **a** reflectivity $R(\omega)$, **b** optical conductivity $\sigma(\omega)$, **c** refractive index $n(\omega)$ and **d** extinction coefficient $k(\omega)$ for $ACuSe_2$.

increasing from the values of 3.5, 3.1 and 3.3 to get the maximum value at the energy values of 1.3, 2 and 2.1 eV for $ScCuSe_2$, $YCuSe_2$ and $LaCuSe_2$, respectively. Then, it decreases to get a value below 1.0 for the energy range of 8.0–13.5 eV. That is due to the group velocity of the incident radiation ($v_g = c/n$), which was greater than the speed of light, c (3.10^8 m/s), for all the three materials. In addition to the mentioned parameters, we calculated the extinction coefficient $k(\omega)$, as shown in Fig. 5d. We observe a sharp increasing for the three spectra from 1 eV to reach the maximum value of k (0), begins at 1.2 eV. Then, it starts increasing when the energy increases until reached the maximum value of 2.2 (3.8 eV), 2.0 (5.5 eV) and 2.2 (5.5 eV) for $ScCuSe_2$, $YCuSe_2$ and

$LaCuSe_2$, respectively. After that, the spectra decrease hardly.

Thermoelectric properties

The electron transport properties are based on the band structure, and they were calculated with the use of semiclassical transfer theory of Boltzmann and solid rigid band theory, as applied in the BoltzTrap code. Thermoelectric compounds are of great importance for renewable energy device applications because heat energy is lost in many energy generation and consumption devices. The best thermoelectric material has a small electrical to thermal conductivity ratio in order to enhance the efficiency
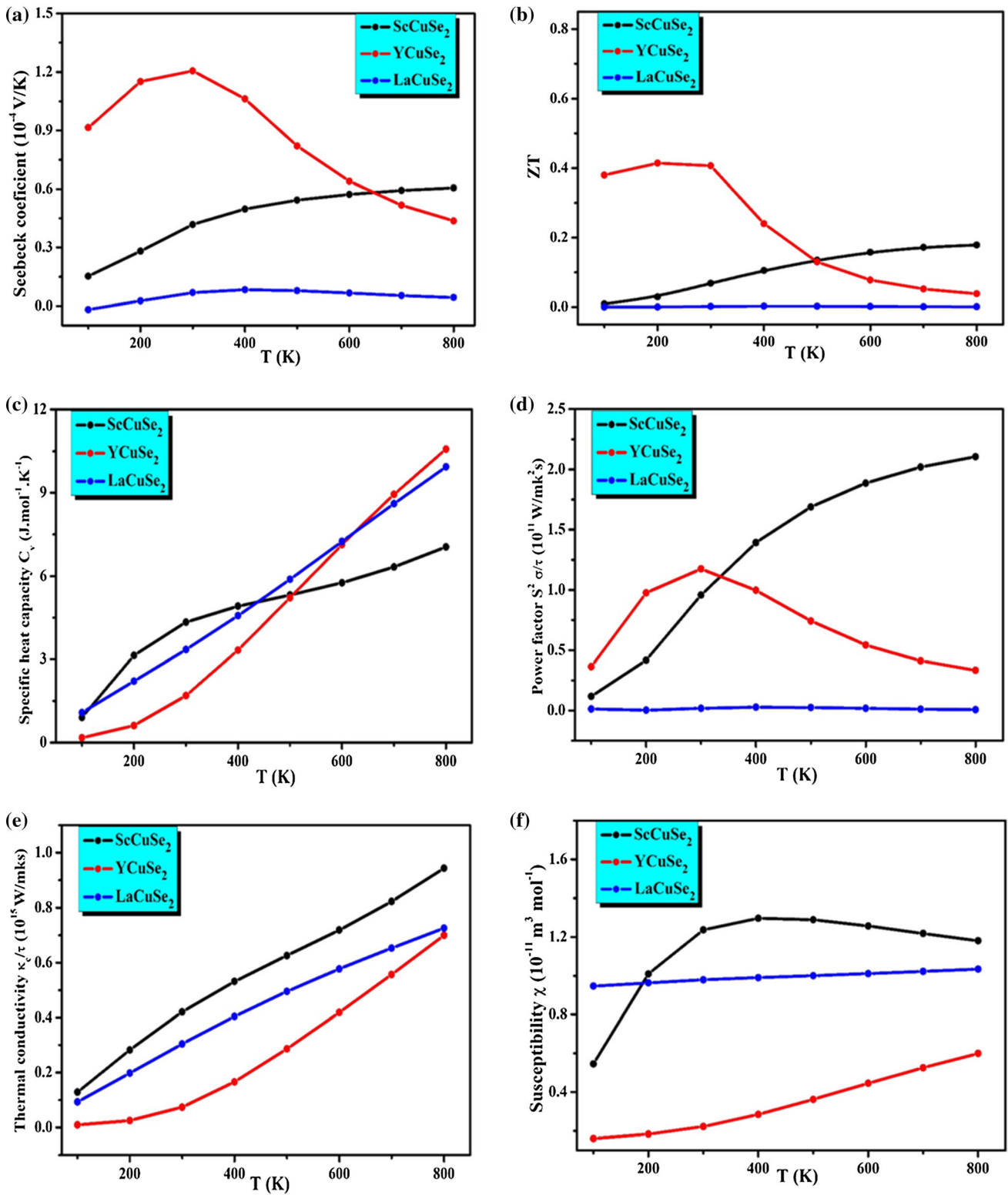
Figure 6 Calculated thermoelectric proprieties as a function of temperature: **a** the Seebeck coefficient, **b** figure of merit, **c** specific heat capacity, **d** power factor, **e** thermal conductivity and **f** susceptibility.

of the devices. Indeed, devices based on these materials exhibit a variety of advantages, including low level of noise, high reliability, lack of moving parts and long service life. To understand the

thermoelectric behavior for the examined materials, we have calculated their thermoelectric proprieties in the temperature range of 0–800 K. In Fig. 6, we show Seebeck coefficient S, figure of merit ZT, specific heat capacity C_v, power factor $S^2\sigma/\tau$, thermal conductivity κ_e/τ and susceptibility χ as a function of temperature. The temperature-dependent Seebeck coefficient is shown in Fig. 6a. For YCuSe$_2$, it increases with temperature to reach the maximum value of 1.38×10^{-4} V/K at room temperature, and then it starts decreasing to attain the minimum value of 0.43×10^{-4} V/K at 800 K. For ScCuSe$_2$, the Seebeck coefficient increases hardly to get the maximum value of 0.6×10^{-4} V/K at 800 K. In LaCuSe$_2$, it increases to reach the maximum at 0.84×10^{-3} V/K at 400 K and then starts decreasing slowly until 800 K. The maximum of the Seebeck coefficient moves to high temperatures on the change of Y to La and Sc, respectively.

The efficiency of thermoelectric materials is estimated also by the parameter of the thermoelectric figure of merit ZT $= S^2\sigma T/\kappa$, where S is the Seebeck coefficient, σ is the electrical conductivity and κ is the thermal conductivity. As clear from Fig. 6b for ScCuSe$_2$, ZT starts increasing with temperature to reach the maximum value of 0.18 at 800 K. In YCuSe$_2$, we observe a sharp increasing from 100 to 200 K where ZT attain a high value of 0.45 at 300 K and then starts decreasing. In LaCuSe$_2$, the maximum value of ZT is at 100 K and then we see a small decreasing with temperature. The maximum of ZT moves to high temperatures on the change of Y to La and Sc. The evolution of ZT with temperature is similar to that of the Seebeck coefficient in agreement with the formula of ZT which is proportional S^2.

Moreover, to understand the behavior of the lattice vibrations, we calculated the specific heat capacity C_v, as shown in Fig. 6c. As seen, C_v increases with temperature for the three materials except for the ScCuSe$_2$, which show a hard increasing. Thus, YCuSe$_2$ and LaCuSe$_2$ have greater specific heat capacity values, as compared to ScCuSe$_2$ material. In fact, the heat capacity increases as T3 at low temperatures until 400 K, reaches the inflexion point at 500 K and then moves toward the saturation at 25 J mol^{-1} K^{-1} (Dulong and Petit law). To study the materials efficiency, we calculated the power factor (PF). The used formula is PF $= S^2 \sigma/\tau$, and it identifies the capability of a compound to yield electricity. As shown in Fig. 6d for LaCuSe$_2$, the PF is still

constant, while ScCuSe$_2$ shows a strong increase with temperature to reach the high value of 2.1×10^{11} W/mk^{2}s at 800 K, and it indicates that it is a valuable material for thermoelectric applications. For YCuSe$_2$, the PF increases with increasing temperature to attain the maximum value of 1.17×10^{11} W/mk^{2}s at 300 K and then it starts decreasing. Thermal conductivity is the ability of a material to conduct heat, and it is determined by phonons and charge carriers. As seen in Fig. 6e, the thermal conductivity increases with rise in temperature. The calculated values of S at 800 K are 9×10^{14}, 7×10^{14} and 7.2×10^{14} (W/mKs) for ScCuSe$_2$, YCuSe$_2$ and LaCuSe$_2$, respectively. The susceptibility of the three examined materials is plotted in Fig. 6f, which describes the material magnetic response. In the case of ScCuSe$_2$, it increases with increasing temperature to reach the maximum value of 1.3×10^{-11} m^3 mol^{-1}, and then it starts decreasing until 800 K. For YCuSe$_2$, it starts increasing from 0.16×10^{-11} at 100 K to 0.6×10^{-11} m^3 mol^{-1} at 800 K, while for LaCuSe$_2$, it nearly remains constant at the value of 10^{-11} m^3 mol^{-1}. When the temperature increases, the susceptibility increases from an initial value to a maximum and then it decreases which is the classical evolution as in the case of ScCuSe$_2$. This investigation of thermoelectric proprieties shows that the examined materials exhibit large Seebeck coefficients, especially of ScCuSe$_2$ and YCuSe$_2$, and it confirms that they are highly efficient thermoelectric materials.

Conclusion

In the present work, the electronic, optical and thermoelectric properties of rare-earth copper selenides chalcogenides ACuSe$_2$ (A = Sc, Y and La) compounds have been explored using FP-LAPW method implemented in the Wien2k code. The electronic band structures calculated with the accurate mBJ approach show that the studied materials are wide band gap semiconductors. Their obtained fundamental gaps are 0.7, 1.2 and 0.8 eV for ScCuSe$_2$, YCuSe$_2$ and LaCuSe$_2$, respectively. ScCuSe$_2$ and YCuSe$_2$ have indirect band gaps along Γ-M direction, whereas LaCuSe$_2$ displays a direct band type transition at the Γ-point. We computed the total density of states (TDOS) and atomic-projected density of states (PDOS) for the studied compounds. The TDOS for the three materials is nearly similar due to the

similarity in chemical bonding. The values of the dielectric constants for the three materials have an inverse relationship with their corresponding band gap because of the negative energy ranges. The computed reflectivity spectra $R(\omega)$ for the three materials have the zero frequency limits at 0.31, 0.25 and 0.29 for $ScCuSe_2$, $YCuSe_2$ and $LaCuSe_2$, respectively, with the maximum peaks in energy range of 7.2–9.4 eV. The sharp peaks of $ScCuSe_2$ and $YCuSe_2$ show that these materials can be used as shielding materials against the UV radiations. The dispersive refractive index $n(\omega)$ increases from 3.5, 3.1 and 3.3 to the maximum values of 4.4,4 and 4.1 at the short infrared and visible wavelengths in $ScCuSe_2$, $YCuSe_2$ and $LaCuSe_2$, respectively. The increasing values of power factor and the figure of merit ZT with temperature show that the $ScCuSe_2$ and $YCuSe_2$ materials are suitable for thermoelectric applications. Finally, we conclude that $ScCuSe_2$ and $YCuSe_2$ are expected to be potential candidates for thermoelectric device applications. This work sheds light on the optoelectronic and thermoelectric properties of $ACuSe_2$ ternary compounds and could offer valuable guidance for the thermal management of copper selenides chalcogenides-based nanoelectronics devices.

Declarations

Conflict of interest The authors have no conflict of interest to declare.

References

[1] Reaver NGF, Khare SV (2014) Imminence of peak in US coal production and overestimation of reserves. Int J Coal Geol 131:90–105. https://doi.org/10.1016/j.coal.2014.05.013

[2] Biswas KA (2015) Advances in thermoelectric materials and devices for energy harnessing and utilization. Proc Indian Natn Sci Acad 81:903–913

[3] Bonnet D, Meyers P (1998) Cadmium-telluride—Material for thin film solar cells. J Mater Res 13:2740–2753. https://doi.org/10.1557/JMR.1998.0376

[4] Başol BM, Kapur VK, Halani A, Leidholm C (1993) Copper indium diselenide thin film solar cells fabricated on flexible foil substrates. Sol Energ Mater Sol Cells 29:163–173. https://doi.org/10.1016/0927-0248(93)90074-D

[5] Meyer BK, Polity A, Reppin D et al (2012) Binary copper oxide semiconductors: from materials towards devices. Phys Status Solidi Basic Res 249:1487–1509. https://doi.org/10.1002/pssb.201248128

[6] Ruhle S, Anderson AY, Barad HN, Kupfer B, Bouhadana Y, Rosh-Hodesh E, Zaban A (2012) All-oxide photovoltaics. J Phys Chem Lett 3:3755–3764

[7] Hoppe H, Sariciftci NS (2004) Organic solar cells: an overview. J Mater Res 19:1924–1945. https://doi.org/10.1557/JMR.2004.0252

[8] Wei J, Yang L, Ma Z et al (2020) Review of current high-ZT thermoelectric materials. J Mater Sci 55:12642–12704. https://doi.org/10.1007/s10853-020-04949-0

[9] Guan M, Zhao K, Qiu P et al (2019) Enhanced thermoelectric performance of quaternary Cu 2–2 x Ag 2 x Se 1–x S x liquid-like chalcogenides. ACS Appl Mater Interfaces 11:13433–13440. https://doi.org/10.1021/acsami.9b01643

[10] Fillet R, Nicolas V, Fierro V, Celzard A (2021) A review of natural materials for solar evaporation. Sol Energ Mater Sol Cells 219:110814. https://doi.org/10.1016/j.solmat.2020.110814

[11] Doolin AJ, Charles RG, De Castro CSP et al (2021) Sustainable solvent selection for the manufacture of methylammonium lead triiodide (MAPbI3) perovskite solar cells. Green Chem 23:2471–2486. https://doi.org/10.1039/d1gc00079a

[12] Dokouzis A, Bella F, Theodosiou K et al (2020) Photoelectrochromic devices with cobalt redox electrolytes. Mater Today Energ 15:100365. https://doi.org/10.1016/j.mtener.2019.100365

[13] Galliano S, Bella F, Bonomo M et al (2020) Hydrogel electrolytes based on xanthan gum: green route towards stable dye-sensitized solar cells. Nanomaterials 10:1–19. https://doi.org/10.3390/nano10081585

[14] Dughaish ZH (2002) Lead telluride as a thermoelectric material for thermoelectric power generation. Phys B Condens Matter 322:205–223. https://doi.org/10.1016/S0921-4526(02)01187-0

[15] Christensen M, Johnsen S, Iversen BB (2010) Thermoelectric clathrates of type I. Dalt Trans 39:978–992. https://doi.org/10.1039/b916400f

[16] Schäfer MC, Bobev S (2013) Tin clathrates with the type II structure. J Am Chem Soc 135:1696–1699. https://doi.org/10.1021/ja3112934

[17] Yin Y, Tudu B, Tiwari A (2017) Recent advances in oxide thermoelectric materials and modules. Vacuum 146:356–374. https://doi.org/10.1016/j.vacuum.2017.04.015

[18] Feng Z, Wu Z, Hua Y, Zhu G, Chen X, Huang S (2021) Controlled growth of perovskite $KMnF_3$ upconverting nanocrystals for near-infrared light-sensitive perovskite solar cells and photodetectors. J Mater Sci 56:14207–14221. https://doi.org/10.1007/s10853-021-06173-w

[19] Wang-yu X, Wang-juan H, Xiang B et al (2019) Attaining reduced lattice thermal conductivity and enhanced electrical conductivity in as-sintered pure n-type Bi_2Te_3 alloy. J Mater Sci 54:4788–4797. https://doi.org/10.1007/s10853-018-3172-9

[20] Mitchell K, Ibers JA (2002) Rare-earth transition-metal chalcogenides. Chem Rev 102:1929–1952. https://doi.org/10.1021/cr010319h

[21] Kim J, Hughbanks T (2000) Synthesis and structures of new ternary aluminum chalcogenides: LiAlSe2, α-LiAlTe2, and β-LiAlTe2. Inorg Chem 39:3092–3097. https://doi.org/10.1021/ic000210c

[22] Isaenko L, Yelisseyev A, Lobanov S et al (2003) Growth and properties of LiGaX2 (X = S, Se, Te) single crystals for nonlinear optical applications in the mid-IR. Cryst Res Technol 38:379–387. https://doi.org/10.1002/crat.200310047

[23] Isaenko L, Vasilyeva I, Merkulov A et al (2005) Growth of new nonlinear crystals L_iMX_2 (M=Al, In, Ga; X=S, Se, Te) for the mid-IR optics. J Cryst Growth 275:217–223. https://doi.org/10.1016/j.jcrysgro.2004.10.089

[24] Kosobutsky AV, Basalaev YM (2010) First principles study of electronic structure and optical properties of L_iMTe_2 (M=Al, Ga, In) crystals. J Phys Chem Solids 71:854–861. https://doi.org/10.1016/j.jpcs.2010.03.033

[25] Andreev YM, Atuchin VV, Lanskii GV et al (2005) Linear optical properties of $LiIn(S_{1-x}Se_x)_2$ crystals and tuning of phase matching conditions. Solid State Sci 7:1188–1193. https://doi.org/10.1016/j.solidstatesciences.2005.05.005

[26] Atuchin VV, Kidyarov BI, Pervukhina NV (2006) Systematic and design of noncentrosymmetric sulfides and selenides for nonlinear optics. Comput Mater Sci 37:507–511. https://doi.org/10.1016/j.commatsci.2005.12.001

[27] Atuchin VV, Kesler VG, Ursaki VV, Tezlevan VE (2006) Electronic structure of $HgGa_2S_4$. Solid State Commun 138:250–254. https://doi.org/10.1016/j.ssc.2006.02.026

[28] Sachanyuk VP, Parasyuk OV, Fedorchuk AO et al (2007) The system Ag_2Se-Ho_2Se_3 in the 0–50 mol.% Ho_2Se_3 range and the crystal structure of two polymorphic forms of $AgHoSe_2$. Mater Res Bull 42:1091–1098. https://doi.org/10.1016/j.materresbull.2006.09.012

[29] Atuchin VV, Liang F, Grazhdannikov S et al (2018) Negative thermal expansion and electronic structure variation of chalcopyrite type L_iGaTe_2. RSC Adv 8:9946–9955. https://doi.org/10.1039/c8ra01079j

[30] Khare IS, Szymanski NJ, Gall D, Irving RE (2020) Electronic, optical, and thermoelectric properties of sodium pnictogen chalcogenides: a first principles study. Comput Mater Sci 183:109818. https://doi.org/10.1016/j.commatsci.2020.109818

[31] Yang KJ, Son DH, Sung SJ et al (2016) A band-gap-graded CZTSSe solar cell with 12.3% efficiency. J Mater Chem A 4:10151–10158. https://doi.org/10.1039/c6ta01558a

[32] Bi J, Ao J, Jeng MJ et al (2017) Three-step vapor Se/N_2-/vapor Se reaction of electrodeposited Cu/In/Ga precursor for preparing $CuInGaSe_2$ thin films. Sol Energ Mater Sol Cells 159:352–361. https://doi.org/10.1016/j.solmat.2016.09.026

[33] Sengar BS, Garg V, Kumar A et al (2018) Band alignment of Cd-free (Zn, Mg)O layer with $Cu_2ZnSn(S, Se)_4$ and its effect on the photovoltaic properties. Opt Mater 84:748–756. https://doi.org/10.1016/j.optmat.2018.08.017

[34] Sengar BS, Garg V, Siddharth G, Kumar A, Pandey SK, Dubey M et al (2021) Improving the $Cu_2ZnSn(S, Se)_4$-based photovoltaic conversion efficiency by back-contact modification. IEEE Trans Electron Devices 68:2748–2752

[35] Sadewasser S, Salomé PMP, Rodriguez-Alvarez H (2017) Materials efficient deposition and heat management of $CuInSe_2$ micro-concentrator solar cells. Sol Energ Mater Sol Cells 159:496–502. https://doi.org/10.1016/j.solmat.2016.09.041

[36] Heinemann MD, Ruske F, Greiner D et al (2016) Advantageous light management in $Cu(In, Ga)Se_2$ superstrate solar cells. Sol Energ Mater Sol Cells 150:76–81. https://doi.org/10.1016/j.solmat.2016.02.005

[37] Cheng Y, Wei K, Xia P, Bai Q (2015) The structural and electronic properties of $Cu(In_{1-x}B_x)Se_2$ as a new photovoltaic material. RSC Adv 5:85431–85435. https://doi.org/10.1039/c5ra13379c

[38] Cheng KW, Hinaro K, Antony MP (2016) Photoelectrochemical water splitting using $Cu(In, Al)Se_2$ photoelectrodes developed via selenization of sputtered Cu-In-Al metal precursors. Sol Energ Mater Sol Cells 151:120–130. https://doi.org/10.1016/j.solmat.2016.03.006

[39] Barkhouse DAR, Gunawan O, Gokmen T et al (2015) Yield predictions for photovoltaic power plants: empirical validation, recent advances and remaining uncertainties. Prog Photovolt Res Appl 20:6–11. https://doi.org/10.1002/pip

[40] Kavitha B, Dhanam M (2013) Structural, photoelectrical characterization of Cu(InAl)Se2 thin films and the fabrication of Cu(InAl)Se2 based solar cells. Electron Mater Lett 9:25–30. https://doi.org/10.1007/s13391-012-2118-7

[41] Kawano K, Hong BC, Sakamoto K et al (2009) Improvement of the conversion efficiency of solar cell by rare earth ion. Opt Mater 31:1353–1356. https://doi.org/10.1016/j.optmat.2008.10.012

[42] Lian H, Hou Z, Shang M et al (2013) Rare earth ions doped phosphors for improving efficiencies of solar cells. Energy 57:270–283. https://doi.org/10.1016/j.energy.2013.05.019

[43] Scanlon DO, Watson GW (2010) Stability, geometry, and electronic structure of an alternative I-III-VI2 material,

CuScS$_2$: a hybrid density functional theory analysis. Appl Phys Lett 97:2008–2011. https://doi.org/10.1063/1.3491179

[44] Brik MG (2013) First-principles calculations of the structural, electronic, optical and elastic properties of the CuYS$_2$ semiconductor. J Phys Condens Matter 25:345802. https://doi.org/10.1088/0953-8984/25/34/345802

[45] Ijjaali I, Mitchell K, Ibers JA (2004) Preparation and structure of the light rare-earth copper selenides LnCuSe$_2$ (Ln=La, Ce, Pr, Nd, Sm). J Solid State Chem 177:760–764. https://doi.org/10.1016/j.jssc.2003.09.007

[46] Li S, Ma R, Zhang X et al (2017) Copper yttrium selenide: a potential photovoltaic absorption material for solar cells. Mater Des 118:163–167. https://doi.org/10.1016/j.matdes.2017.01.037

[47] Rugut E, Joubert D, Jones G (2019) Lattice dynamics and thermoelectric properties of YCuSe$_2$. Mater Today Commun 21:1–7. https://doi.org/10.1016/j.mtcomm.2019.100617

[48] Julien-Pouzol M, Guittard M (1972) Étude cristallochimique des combinaisons ternaries cuivre-terre rare soufre ou Sélenium, siyuées le long des binares Cu$_2$X–L$_2$X$_3$. Ann Chim, 7: 253–262

[49] Hasnip PJ, Refson K, Probert MIJ et al (2014) Density functional theory in the solid state. Philos Trans R Soc A Math Phys Eng Sci 372:20130270. https://doi.org/10.1098/rsta.2013.0270

[50] Khyzhun OY, Bekenev VL, Atuchin VV et al (2013) Electronic properties of ZnWO$_4$ based on ab initio FP-LAPW band-structure calculations and X-ray spectroscopy data. Mater Chem Phys 140:588–595. https://doi.org/10.1016/j.matchemphys.2013.04.010

[51] Ji H, Huang Z, Xia Z et al (2015) Comparative investigations of the crystal structure and photoluminescence property of eulytite-type Ba$_3$Eu(PO4)$_3$ and Sr$_3$Eu(PO4)$_3$. Dalt Trans 44:7679–7686. https://doi.org/10.1039/c4dt03887h

[52] Reshak AH, Alahmed ZA, Bila J et al (2016) Exploration of the electronic structure of monoclinic α-Eu$_2$(MoO$_4$)$_3$: DFT-based study and X-ray photoelectron spectroscopy. J Phys Chem C 120:10559–10568. https://doi.org/10.1021/acs.jpcc.6b01489

[53] Carella A, Centore R, Borbone F et al (2018) Tuning optical and electronic properties in novel carbazole photosensitizers for p-type dye-sensitized solar cells. Electrochim Acta 292:805–816. https://doi.org/10.1016/j.electacta.2018.09.204

[54] Atuchin VV, Vinnik DA, Gavrilova TA et al (2016) flux crystal growth and the electronic structure of BaFe12O19 hexaferrite. J Phys Chem C 120:5114–5123. https://doi.org/10.1021/acs.jpcc.5b12243

[55] Denisenko YG, Atuchin VV, Molokeev MS et al (2021) Negative thermal expansion in one-dimension of a new double sulfate AgHo(SO4)$_2$ with isolated SO$_4$ tetrahedra. J Mater Sci Technol 76:111–121. https://doi.org/10.1016/j.jmst.2020.10.026

[56] Blaha, P, Schwarz, K, Madsen, GK, Kvasnicka, D, Luitz J (2001) An Augmented Plane Wave+ Local Orbitals Program for Calculating Crystal Properties 60

[57] Perdew JP, Zunger A (1981) Self-interaction correction to density-functional approximations for many-electron systems. Phys Rev B 23:5048–5079. https://doi.org/10.1103/PhysRevB.23.5048

[58] Camargo-Martínez JA, Baquero R (2012) Performance of the modified Becke-Johnson potential for semiconductors. Phys Rev B Condens Matter Mater Phys 86:1–8. https://doi.org/10.1103/PhysRevB.86.195106

[59] Baizaee SM, Mousavi N (2009) First-principles study of the electronic and optical properties of rutile TiO$_2$. Phys B Condens Matter 404:2111–2116. https://doi.org/10.1016/j.physb.2009.01.014

[60] Madsen GKH, Carrete J, Verstraete MJ (2018) BoltzTraP2, a program for interpolating band structures and calculating semi-classical transport coefficients. Comput Phys Commun 231:140–145. https://doi.org/10.1016/j.cpc.2018.05.010

[61] Shemet V, L. Gulay LO, (2005) Isothermal sections of the Y$_2$Se$_3$-Cu$_2$Se-Sn (Pb) Se systems at 870 K and crystal structure of the Y4. 2Pb0.7Se7 compound. Pol J Chem 79:1315–1326

[62] Julien-Pouzol M, Jaulmes S, Mazurier A, Guittard M (1981) Structure du disulfure de lanthane et de cuivre. Acta Crystallogr Sect B Struct Crystallogr Cryst Chem 37:1901–1903

[63] Mehl MJ, Klein BM, Papaconstantopoulos DA (1995) Intermetallic compounds: principle and practice. Principles 1:195–210

Springer